Coupled Systems Mechanics, *Vol. 3, No. 1 (2014) 27-52*
DOI: http://dx.doi.org/10.12989/csm.2014.3.1.027

Modeling of coupled THMC processes in porous media

Ursula Kowalsky*, Sonja Bente[a] and Dieter Dinkler[b]

Institute for Structural Analysis, TU Braunschweig, Beethovenstraße 51, 38106 Braunschweig, Germany

(Received January 11, 2014, Revised March 10, 2014, Accepted March 15, 2014)

Abstract. For landfill monitoring and aftercare, long-term prognoses of emission and deformation behaviour are required. Landfills may be considered as heterogeneous porous soil-like structures, in which flow and transport processes of gases and liquids interact with local material degradation and mechanical deformation of the solid skeleton. Therefore, in the framework of continuous porous media mechanics a model is developed that permits the investigation of coupled mechanical, hydraulical and biochemical processes in municipal solid waste landfills.

Keywords: multiphysics; porous media; waste; transport processes; degradation; settlements

1. Introduction

Waste is a heterogeneous material with complex properties. The observable phenomena can be split up into three major parts: mechanical, hydraulical and biochemical processes. All of them influence each other directly or indirectly, which makes any quantitative prognosis for settlements, gas generation, leachate characteristics or landfill body stability difficult, see Fig. 1.

An important question is, e.g., to which extent the loss of solid matter is transferred to additional settlement. Municipal solid waste consists of a deformable, bio-degradable solid skeleton and a porespace, which is filled with liquid and gaseous phases. High loadings together with a high water saturation and a low permeability of the material might lead to excess pore pressures,which may reduce the effective stresses, that are beared by the solid skeleton, and thus the deformation.

In addition, short-time settlements increase with time due to consolidation. At a larger time scale, creep of the material itself or compression of micropores causes additional deformations. Furthermore, long-time settlements might occur due to biochemical processes, since waste decomposes mainly under anaerobic conditions via several stages to methane, carbon dioxide, water and acids. Simultaneously, biomass grows and decreases due to the degradation of organic matter. Reaction rates are influenced by environmental conditions like water content, temperature and pH. Generated heat is transported convectively via pore water and gas and by thermal conduction. Temperature affects the activity of bio mass and thus the degradation rates and the

*Corresponding author, Dr.-Ing., E-mail: u.kowalsky@tu-bs.de
[a] Dr.-Ing., E-mail: sonja-bente@gmx.eu
[b] Professor Dr.-Ing., E-mail: d.dinkler@tu-bs.de

http://www.techno-press.org/?journal=csm&subpage=7 ISSN: 2234-2184 (Print), 2234-2192 (Online)

viscosity of the fluid phases. Both leachate and landfill gas can move through the pore space of the porous medium. The two phases are immiscible, whereas leachate represents the wetting phase and the landfill gas the non-wetting phase. Due to the loss of solid matter caused by biological degradation the density of the material changes. Since deformation changes porosity and permeability, reactions will be affected indirectly by transport processes.

The development of mathematical models for landfill behaviour starts with models for single processes. Areas of interest are especially the gas production of landfills, surface settlements and water balance. More advanced models concentrate both on a refinement of the description of single processes itself, for example a more detailed reaction scheme, and on coupling of different processes that are considered isolated before.

Several one-dimensional approaches exist to describe the time-settlement behaviour of waste. Some are based on a mathematical description of the evolution of successive stages but not of the mechanisms, which cause the compaction. Time-dependent parameters are determined by fitting numerical results to experimental measurements. Models sometimes assume a linear relationship between settlement and logarithm of time, e.g., in the approach by Wall and Zeiss (1995) who investigate the relation of degradation and settlement in lysimeters. Primary and secondary settlements may be described by two compression coefficients that correspond to the slopes of a bilinear time-settlement curve in semi-logarithmic scale. A basic approach often is to assume that secondary settlement follows the kinetics of biological degradation. Thus, models for secondary settlement are often derived from first order kinetics, as for example in the models by Park and Lee (2002), Oweis (2006), Hettiarachchi *et al*. (2007) or Simoes and Da Silva (2011). For an overview on settlement models the reader may be referred to Elagroudy *et al*. (2008), El Fadel and Khoury (2000) and Ivanova (2007).

As part of more advanced models, degradation induced settlements are coupled with transport and degradation processes. MODUELO is a three-dimensional model developed at the University of Cantabria. The first version consists of a module for the hydraulic behavior, see Garcia de Cortazar *et al*. (2002a), and a model for degradation, see Garcia de Cortazar*et al*. (2002b). The model is able to reproduce the filling history of a landfill site. Besides moisture storage and transport, the water balance of each cell includes precipitation, surface runoff and evaporation. In MODUELO3, a settlement model is included, which describes degradation induced settlements by the ratio of relative settlement to relative mass loss, see Lobo *et al*. (2008).

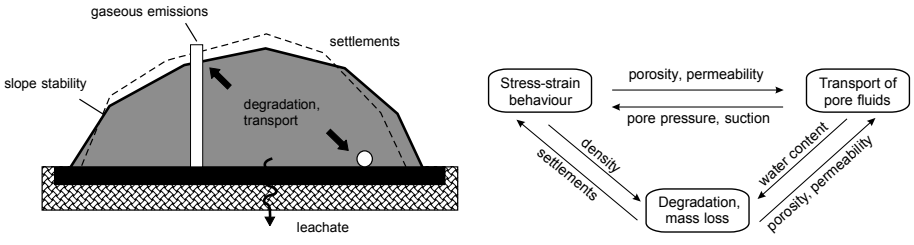

Fig. 1 Processes in MSW landfills – interactions considered

The model HBM presented by McDougall (2007) couples hydraulical processes, degradation and mechanical behaviour within a staggered solution procedure. The Cam Clay model is used to describe inelastic deformations. To investigate how solid mass loss caused by biodegradation is transferred into settlements, a void change parameter is introduced. It describes loosening and densification during degradation and the influence on combined isotropic and kinematic hardening. The model LDAT, White (2008), couples degradation of waste including leachate chemistry with liquid and gas transport and settlements. Settlements are calculated by relating dry density and effective stress. The relation is empirically derived by Powrie and Beaven (1999).

Machado *et al*. (2008) pick up the work by McDougall (2007) and consider the effect of degradation on settlements in a similar manner by applying a void change parameter. The parameter is assumed to be proportional to degraded solid waste mass, which is described by a first order decay model. A novel aspect is to take into account the influence of changes in the fibrous fraction on the mechanical strength properties of municipal solid waste.

One of the first approaches of coupling the major phenomena in a strong, simultaneous solution scheme instead in a staggered procedure is presented by Ricken and Ustohalova (2005) and Ustohalova *et al*. (2006). A modified version of the model is later published under the name DepSim. The tri-phase model is developed within the Theory of Porous Media, whereas its thermodynamic consistency is proven by fulfilling the entropy inequality. Applications of the model are presented by Ricken *et al*. (2009).

Durmusoglu *et al*. (2005) present a multiphase model which couples gas production with liquid and gas flow according to Darcy's law considering capillary effects. Time-dependent deformation is modelled using Maxwell's rheology. A Bishop-type effective stress is used. To the authors' knowledge, this is, besides the model presented in this paper, the only model for MSW, which includes an effective stress concept for unsaturated conditions. The balance equations are solved by means of the Finite Element Method in one dimension.

Yu *et al*. (2009) develop a model for analysing the gas flow to a gas extraction well in a deformable landfill. Mechanical behaviour is described by a series connection of a Hooke and a Kelvin element. The rheological element enables description of primary and secondary settlements. The constitutive law for compression is coupled with the gas balance. Yu *et al*. assume isothermal conditions, constant porosity and saturation as well as constant degradation rates and gas conductivity of the waste. Numerical results are compared with an analytical solution and with field measurements of gas flux and settlement.

2. Multiphysics framework for modeling coupled processes

The presented model treats municipal solid waste as a continuum within the Theory of Porous Media, see for example de Boer (2005) or Lewis and Schrefler (1998). It is based on the Theory of Mixtures, see for example Bowen (1976), whereas the portions of the mixture's constituents are restricted by the Concept of Volume Fractions. The constituents are homogenised over a control volume, which is termed Representative Elementary Volume, REV. The REV determines the scale of uniform properties and does in general not coincide with any numerical discretisation. All constituents simultaneously exist with their volume fraction at a given spatial point. This approach is also termed superimposed continua. A prerequisite is that the homogenisation process is possible and valid for description of the selected phenomena and material properties.

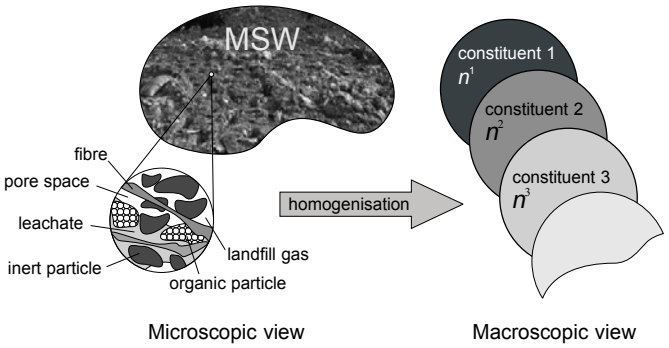

Fig. 2 Microscopic view at waste material and virtual homogenisation

As indicated, municipal solid waste is a porous material consisting of a solid skeleton and a pore space. The microscopic view in Fig. 2 visualises that the solid phase consists of several components. According to the shape of the solid particles, granular, soil-like particles can be distinguished from elongate, fibrous particles. Furthermore, the solid matter may be divided with respect to biological degradability, so that inert matter, organic matter and biomass are distinguished in general. Two fluid phases, leachate and landfill gas, fill the pore space. Both fluid phases contain several chemical substances, whereas the composition changes due to ongoing degradation and physical exchange processes.

The constituents α of the waste mixture are divided both into components β and phases π. The term phase is related to the aggregate state, components are the substances which form the phases. Thus, the components themselves belong to distinct phases whereas also phase changes are possible. Due to the homogenisation, the discrete distribution of all constituents may remain unknown. Each of them is considered only by its volume fraction n^α on the macroscopic scale, see Fig. 2.

The developed model considers three phases: one solid (s) and two fluid phases, namely liquid (l) and gas (g). The components of each phase are dependent on the detailedness of the constitutive model. Each constituent α, each phase π and each component β occupy a certain volume dv^α, dv^π and dv^β. The particular volume fractions n^α, n^π and n^β are defined by

$$n^\alpha = \frac{dv^\alpha}{dv},\ n^\beta = \frac{dv^\beta}{dv} \text{ and } n^\pi = \frac{dv^\pi}{dv} \tag{1}$$

The saturation constraint requires that the sum of all volume fractions is equal to unity.

$$\sum_\alpha n^\alpha = 1 \text{ and} \sum_\beta n^\beta = 1 \text{ and} \sum_\pi n^\pi = 1 \tag{2}$$

The sum of the volume fractions of the fluid phases is related to the porosity ϕ, which is the fraction of the pore volume dv^p and defined by

$$\phi = \frac{dv^l + dv^g}{dv} = \frac{dv^p}{dv} = n^l + n^g = 1 - n^s \tag{3}$$

For $S_l = dv^l/dv = 1$ the porous medium is fully saturated, for $S_l = 0$ the material is dry. Mainly, intermediate states are present in landfills, which are called unsaturated or partially saturated. If the constituents are immiscible, they occupy their own partial volume and different densities can be defined. The intrinsic density or real density $\tilde{\rho}^\alpha$ relates the mass m^α of a constituent α to the volume occupied by the constituent. The partial density ρ^α relates the mass to the total volume, whereas both density measures can be transformed into each other by the volume fraction

$$\tilde{\rho}^\alpha = \frac{m^\alpha}{dv^\alpha} \text{ and } \rho^\alpha = \frac{m^\alpha}{dv} \text{ with } \rho^\alpha = n^\alpha \tilde{\rho}^\alpha \tag{4}$$

The partial density corresponds to the bulk density, whereas both dry and wet density are commonly used in waste management. If the constituent α is incompressible, the intrinsic density is constant, whereas the partial density may still change due to a change in volume fraction. The porosity ϕ is related to the partial density and the intrinsic density of the solid phase by

$$\phi = 1 - \frac{\rho^s}{\tilde{\rho}^s} \tag{5}$$

Based on the Theory of Porous Media, the balance equations of momentum, mass and energy are formulated on the macroscopic level, which implies a volume-coupled formulation.

A weak formulation is developed as basis for the tri-phase model considering a solid, a liquid and a gaseous phase. The balance equations refer to different reference systems. Here, a Lagrangian description of the solid skeleton regarding finite deformations is combined with an Arbitrary Lagrangian-Eulerian description of the fluid phases and their components.

2.1 Principle of Virtual Work for the solid

The Principle of Virtual Work for the weak formulation of equilibrium using large strain kinematics is given by

$$\begin{aligned} &\underbrace{\int_{V_0} \delta\mathbf{E} : (\mathrm{S_e} - \mathbf{F}_s^{-1} \det \mathbf{F}_s \cdot (p_g + S_l \cdot (p_l - p_g) - p_{atm}) \cdot \mathbf{1}) \mathbf{F}_s^{-T}) dV_0}_{\text{virtual internal work}} \\ &= \underbrace{\int_{\Gamma_0} \delta\mathbf{u}\, \mathbf{t}_0\, dS_0}_{\text{work of surface tractions}} + \underbrace{\int_{V_0} \delta\mathbf{u} \rho_{ref}\, \mathbf{g}\, dV_0}_{\text{work of volume loads (self-weight)}} \end{aligned} \tag{6}$$

with the virtual Green's strains $\mathbf{E}$, the effective 2nd Piola-Kirchhoff stresses $\mathbf{S}_e$, the deformation gradient of the solid $\mathbf{F}_S$, pressure of the gas phase p_g and of the liquid phase p_l respectively, the saturation of the liquid phase S_l, the atmospheric pressure p_{atm}, the virtual displacement δu and gravity accelerationg $\mathbf{g}$.

For determination of external virtual work of the self-weight in Total Lagrangian description the density ρ_{ref} with respect to the reference configuration is defined as

$$(\rho_s^{IM} + \rho_s^{DO} + \rho_s^{X} + \rho_l) \cdot \det \mathbf{F}_s = \rho_{ref} \tag{7}$$

The densities ρ^α refer to the solid components, which are inert matter *IM*, degradable organic matter *DO* and biomass, i.e., bacteria genera *X*.

2.2 Weak formulation of mass balances for fluid components

The fluid phases and their components are formulated in Eulerian description. The reference frame is however not fixed, but connected to the solid phase. Thus, the Eulerian frame moves with the solid phase. This represents a special case of an arbitrary Lagrangian-Eulerian description, see for example Donea *et al*. (2004), whereas the movement of the reference frame coincides with the movement of one of the constituents, i.e., the solid skeleton.

In a domain which is free of sources and sinks any change in mass of component α is caused by a flux over the moving boundary of the control volume. Therefore, the rate of change in mass is balanced by the surface fluxes which yields its conservative form

$$\frac{d}{dt}\int_{V(t)} \rho^\alpha dV + \int_{S(t)} \rho^\alpha (\mathbf{v}_\pi - \mathbf{v}_s)\mathbf{n}\, dS = 0 \tag{8}$$

with $\mathbf{v}_\pi$ being the flow speed of fluid phase π, $\mathbf{v}_S$ the surface movement of control volume and $\mathbf{n}$ the outward facing normal vector.

In case of the presented model for waste also sources and sinks due to reactions of physical exchange have to be considered so that the right hand side of Eq. (8) is not equal to zero and thus has to be extended by an additional term r^α, which describes a local rate of change in density due to reactions

$$\frac{d}{dt}\int_{V(t)} \rho^\alpha dV + \int_{S(t)} \rho^\alpha (\mathbf{v}_\pi - \mathbf{v}_s)\mathbf{n}\, dS = \int r^\alpha dV \tag{9}$$

If the surface velocity $\mathbf{v}_s = 0$, the Eulerian representation of the balance equation of mass is obtained, for $\mathbf{v}_s = \mathbf{v}_\pi$ the Lagrangian one. Adding the mass balance equations of all single components yields the mass balance for the whole mixture.

2.3 Weak formulation of balance of energy

Landfills might exhibit high variations in temperature due to the degradation of organic matter, which in turn influences degradation and transport. Thus, the presented model considers the equation for conservation of energy analogously to the mass balance. It is assumed that all constituents keep the thermodynamic equilibrium and got the same temperature. Due to the degradation processes and physical exchange processes the conservation of energy is very complex. Storage terms and convective terms are balanced by sources and sinks due to degradation. The general balance of energy for the whole mixture with the volume-specific energy *e* yields

$$\frac{d}{dt}\int_{V(t)} e\, dV + \sum_\alpha \int_{S(t)} e_\alpha (\mathbf{v}^\alpha - \mathbf{v}^s)\mathbf{n}\, dS = \sum \int r_{e,\alpha}\, dV \tag{10}$$

with a term r_e accounting for sources and sinks.

3. Material equations

The characteristic material behaviour concerning thermal, hydraulical, mechanical and biochemical processes is described by the respective mathematical models, which are presented in this section as detailed as necessary for understanding the procedure to consider the interactions between the single processes and the monolithic algorihm to solve the governing equations.

3.1 Biological degradation and heat generation

Due to the water content at emplacement, subsequent compaction and infiltrating precipitation, degradation proceeds mainly under anaerobic conditions in landfills. Degradation models of varying complexity may be incorporated into the coupled description of THMC processes presented here by mass exchange terms. Respective models are developed e.g., by Haarstrick *et al*. (2001), Kindlein *et al*. (2006) and Reichel and Haarstrick (2008). Krase *et al*. (2009) report the coupling methodology describing stoichiometry, reaction rates and numerical implementation into weak formulation of mass balance by source and sink terms respectively.

Fig. 3 gives an overview of the components that are balanced by the model proposed here, and how they are related by reactions and physical exchange processes. R1, R2 and L refer to the reactions of anaerobic degradation. In the first step R1, organic matter DO reacts with water to acetic acid and carbon dioxide. The reaction is accompanied by the growth of biomass X. In the second step R2 acetic acid reacts to water, carbon dioxide, methane and biomass as well. The step L describes the lysis of biomass, which is in this model a degradation to organic matter considering overall mass conservation. Evaporation, condensation and dissolution are considered as well and denoted by P1 and P2, respectively.

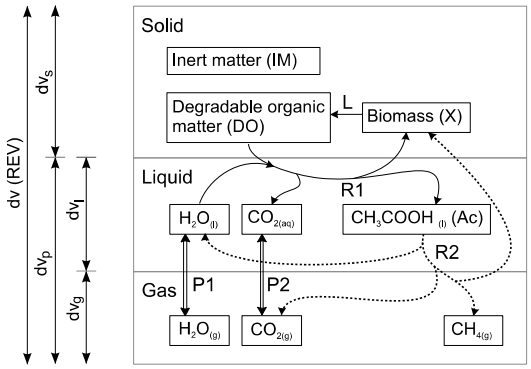

Fig. 3 Overview of biochemical reactions' model

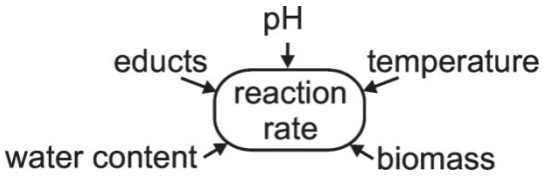

Fig. 4 Factors influencing degradation rates

Decomposition is catalyzed by microbiological growth, which is influenced by growth-limiting substrates. Furthermore, environmental conditions, especially temperature, water content and pH, are supposed to influence the activity of bacteria, see Fig. 4.

Monod (1949) shows that the growth of bacterial cultures may be described by a hyperbolic function so that the rate of change of a substrate S is - in terms of partial density -

$$\dot{\rho}^S = \mu_{\max} \frac{\rho^S}{K^S + \rho^S} \cdot \rho^X \tag{11}$$

whereas μ_{max} is the maximum degradation rate, ρ^S is the density of a limiting substrate S, the Monod constant K^S and ρ^X is the partial density of biomass. For the lysis of biomass, a rate law of first order is assumed. Hence, in detail the rates of the reactions R1, R2 and L are

$$\begin{aligned} R1: \quad & \dot{\rho}^{DO} = \mu_{\max,R1} \frac{\rho^{DO}}{K^{DO} + \rho^{DO}} \cdot \rho^X \cdot f_\Theta \cdot f_{Sl} \cdot f_{pH}, \\ R2: \quad & \dot{\rho}^{Ac} = \mu_{\max,R2} \frac{\rho^{Ac}}{K^{Ac} + \rho^{Ac}} \cdot \rho^X \cdot f_\Theta \cdot f_{Sl} \cdot f_{pH} \\ L: \quad & \dot{\rho}^X = \mu_{\max,L}\, \rho^X \cdot f_{\Theta,L} \end{aligned} \tag{12}$$

The factors f_Θ, f_{Sl} and f_{pH}, varying between zero and one, describe the influence of temperature, water content and pH, respectively. They are given by

$$\begin{aligned} f_\Theta &= f_{\Theta,1} \cdot f_{\Theta,2} \\ f_{\Theta,1} &= e^{-\left[(k_\Theta(\Theta-\Theta_{opt}))^2\right]} \\ f_{\Theta,2} &= \begin{cases} 1 & \text{for } \Theta < \Theta_l \\ \frac{1}{2}(1+\cos\frac{(\Theta-\Theta_l)\pi}{\Theta_h-\Theta_l}), & \text{for } \Theta_l \le \Theta \le \Theta_h \\ 0 & \text{for } \Theta > \Theta_h \end{cases} \end{aligned} \tag{13}$$

The quantities k_Θ, Θ_{opt}, Θ_l and Θ_h are parameters to fit the relation to experimental data, see Table 1.

Table 1 Parameters for temperature functions

	k_Θ (1/°C)	Θ_{opt} (°C)	Θ_l (°C)	Θ_h (°C)
		Set 1		
0.030	57	70	80	
		Set 2		
R1	0.030	20	50	70
R2	0.045	30	42	80

For the lysis of biomass, reaction L, a functional relation is used for f_Θ, with

$$f_{\Theta,L} = e^{k_{\Theta,L}(\Theta-\Theta_{opt,L})} \tag{14}$$

whereas $k_{\Theta,L} = 0.04$ and $\Theta_{opt,L} = 80$°C. For the influence of pH on degradation rate f_{pH}

$$f_{pH=} \frac{K_{pH}}{K_{pH} + \frac{(10^{pH} - 10^{pH_{opt}})^2}{10^{(pH+pH_{opt})}}} \tag{15}$$

is applied with the parameters K_{pH} and pH_{opt}. Moisture content influences degradation rate via nutrient supply. The following function is used

$$f_\omega = 1/2 + \frac{1}{\pi}\arctan\left[(\omega - \omega_{opt})F_W\right] \tag{16}$$

The parameter w_{opt} determines the water content at the inflexion point, whereas F_W determines the steepest slope. Wet moisture content is related to porosity and liquid saturation by

$$\omega_{wet} = \frac{S_l \phi \tilde{\rho}_l}{\rho_s + S_l \phi \tilde{\rho}_l} \tag{17}$$

The biological degradation processes usually lead to heat generation in landfills whereas the processes themselves are temperature dependent. Here, heat generation from exothermic reactions is considered. Generated heat is transported convectively and by thermal conduction. Heat conduction due to a gradient in the temperature field is described by means of Fourier's law which defines the heat flux q (W/m^2) dependent on the thermal conductivity λ_S by

$$\mathbf{q} = -\lambda_s \cdot \operatorname{grad}\Theta \tag{18}$$

Heat capacities are required for determination of stored energy and are listed for different components in Table 2.

Table 2 Heat capacities of employed components (kJ/(kg K))

$C_{p,g}^{H_2O} = 1.80$	$C_{p,l}^{H_2O} = 4.18$	$C_{p,s}^{DO} = 0.8$
$C_{p,g}^{CO_2} = 0.82$	$C_{p,l}^{CO_2} = 4.18$	$C_{p,s}^{IM} = 0.8$
$C_{p,g}^{CH_4} = 2.19$	$C_{p,l}^{AC} = 2.05$	$C_{p,s}^{X} = 0.8$

Data for fluid components taken from NIST
National Institute of Standards and Technology, Chemistry WebBook
http:// webbook.nist.gov/chemistry/, access in December 2009

3.2 Transport properties

Waste is a porous medium with liquid phase and gas phase filling the pore space. Due to drainage, the waste is likely to be unsaturated at most times. The components of the phases are transported with the phase velocity which is termed convective transport. Considering that the fluid phases of MSW are composed of several components, multiphasic, multicomponent transport has to be modeled including description of phase changes. For an overview of transport models the reader may be referred to the reviews by El-Fadel *et al*. (1996a, b).

The observation of preferential flow in experiments on waste indicates special characteristics of the waste's pore structure. Interparticle pore volume may be distinguished from intraparticle space. Correspondingly, the fluid phases in MSW may exist in a free form and in a bounded form, being trapped in closed pores and isolated from the fast convective transport in the larger macropores, see Fig. 5.

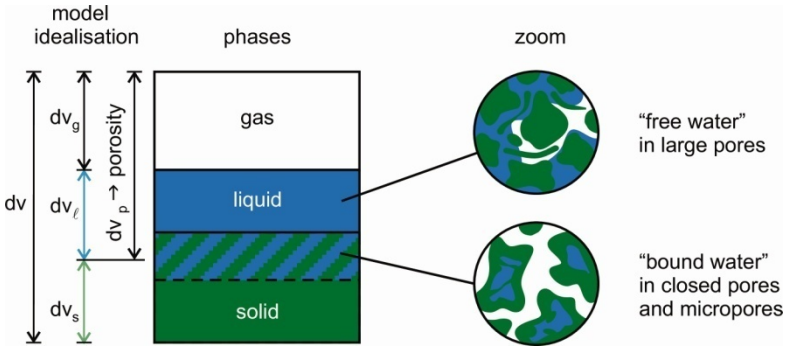

Fig. 5 Model for moisture storage

The intraparticle pore space is attributed to the total pore space, and it is assumed that the solid grains are incompressible. Thus, for the case that no mass exchange with the solid phase occurs, the porosity on the current configuration is dependent on the deformation only and the whole volume change $\Delta v = dv - dV_0$ of a control volume of the mixture results in a corresponding volume change of the pore space. The current porosity can then be derived from the initial porosity Φ_0 to

$$\phi = \frac{dV_0^p + \Delta v}{dV_0 + \Delta v} = \frac{dV_0\phi_0 + dv - dV_0}{dv} = 1 + (\phi_0 - 1)\frac{dV_0}{dv} = 1 + \frac{(\phi_0 - 1)}{\det \mathbf{F}_s} \tag{19}$$

where dV_0 and dV_o^p represent initial volume and initial pore volume, respectively, and where dV is the current volume of a REV. If solid mass loss due to degradation of organic matter is considered as well, the porosity is not directly linked to deformation only. Rather, it is related to partial solid density ρ_s and intrinsic density $\tilde{\rho}_s$ by

$$\phi = \frac{dv - dv_s}{dv} = \frac{dv - \dfrac{\rho_s dv}{\tilde{\rho}_s}}{dv} = \frac{\tilde{\rho}_s - \rho_s}{\tilde{\rho}_s} = 1 - \frac{\rho_s}{\tilde{\rho}_s} \tag{20}$$

The retention of the wetting, liquid phase in open pores is caused by capillary effects, also called matrix suction. Its magnitude depends on the pore size, on the surface tension of the liquid and on the texture of the surface of the pores and often is related to moisture content or saturation, described by the Soil Water Characteristic Curve (SWCC). Two approaches for a SWCC are applied here, the capillary pressure may be defined by Brooks and Corey (1966) or by van Genuchten (1980).

Convective transport of the leachate and the landfill gas are described by means of a generalized Darcy's law, which covers unsaturated flow by introducing relative permeabilities $k_{\pi,rel}$ and dynamic viscosities η_l, details are given in Brooks and Corey (1966), Burdine (1953), van Genuchten (1980) or Mualem (1976). For a liquid and a gas phase, the Darcy velocities and $\mathbf{v}_{g,D}$ within a three-dimensional framework are

$$\begin{aligned} \mathbf{v}_{l.D} &= n_l \mathbf{v}_{ls} = n_l(\mathbf{v}_l - \mathbf{v}_s) = -\frac{k_{l,rel}}{\eta_l}\mathbf{K}(\text{grad } p_l - \tilde{\rho}_l \mathbf{g}), \text{ and} \\ \mathbf{v}_{g.D} &= n_g \mathbf{v}_{gs} = n_g(\mathbf{v}_g - \mathbf{v}_s) = -\frac{k_{g,rel}}{\eta_g}\mathbf{K}(\text{grad } p_g - \tilde{\rho}_g \mathbf{g}) \end{aligned} \tag{21}$$

In general, the permeability $\mathbf{K}$ (m^2) represents an anisotropic tensor quantity. Permeability is related to the hydraulic conductivity $\mathbf{k}_{\pi f}$(m/s) by

$$\mathbf{k}_{\pi,f} = \mathbf{K}\frac{\rho_\pi}{\eta_\pi}g = \mathbf{K}\frac{1}{\nu_\pi}g \Rightarrow \text{ e.g. for liquid at } 20^\circ\text{C } \mathbf{k}_{l,f}(\text{m/s}) = \mathbf{K} \cdot 1 \times 10^7 (\text{m}^2) \tag{22}$$

with kinematic viscosity ν_π, depending on temperature.

The influence of the deformation on the hydraulic properties is considered. Thereby, the effect of compaction on permeability is taken into account by a power law between porosity and permeability

$$\mathbf{K} = \mathbf{K}_0 \cdot \left(\frac{\phi_t}{\phi_0}\right)^{k_\phi} \Rightarrow \mathbf{K} = \left(\frac{\tilde{\rho}_s - \rho_{s,i}}{\tilde{\rho} - \rho_{s,0}}\right)^{k_\phi} \cdot \mathbf{K}_0 \tag{23}$$

Φ_0 and $\mathbf{K}_0$ refer to initial porosity and permeability respectively. The parameter κ covers the deformation dependence. For $\kappa_\phi = 0$ the permeability remains constant, if $\kappa_\phi = 1$ a linear relationship is obtained. It is assumed that the change of permeability is isotropic, i.e., a unique value of κ_ϕ is used for all principal directions. It is proven by experiments that the way of emplacement in thin layers causes an orientation of the particles in horizontal direction leading to an anisotropic permeability, so that the tensor $\mathbf{K}_{loc}$ becomes

$$\mathrm{K}_{loc} = \begin{pmatrix} K_{11} & 0 & 0 \\ 0 & K_{22} & 0 \\ 0 & 0 & K_{33} \end{pmatrix} \tag{24}$$

and the influence of rotation from local to global frame is described by a transformation of local permeability to global permeability with the tensor $\mathbf{R}$

$$\mathbf{K}_{glob} = \mathbf{R} \cdot \mathbf{K}_{loc} \cdot \mathbf{R}^T \tag{25}$$

The rotation tensor $\mathbf{R}$ is formed using the deformation gradient in case of finite strains. If the rotational deformations are small, the tensor $\mathbf{R}$ is set equal to $\mathbf{1}$.

3.3 Physical exchange processes

Some components are considered to exist both in gaseous and in liquid state. The proposed model describes evaporation and condensation of water as well as dissolution of carbon dioxide. Description of saturated vapor pressure and vapor pressure reduction due to capillarity influence the transport characteristics of MSW as well as the evaporation enthalpy has to be considered in dependence on temperature in the balance of energy.

The gas phase is considered to be an ideal gas mixture, whereas the pressure of the gas mixture is equal to the sum of the partial pressures according to Dalton's law, Eq. (26)

$$p^g = \sum_\beta p_g^\beta = p_g^{CH_4} + p_g^{CO_2} + p_g^{H_2O} \tag{26}$$

The dissolution of methane is neglected as its portion is very small. The dissolution of carbon dioxide is described by Henry's law. Assuming equilibrium in the relation of the concentrations in the gas phase and the liquid phase, respectively, Henry's coefficient is derived.

3.4 Effective stress concept

The effective stress is often referred to as being the stress, which controls the mechanical properties, particular shear strength and volume change of the investigated medium and structure. Thus, the material model for the mechanical behaviour is usually formulated in terms of effective stress, which considers the influence of the pore pressures of liquid and gas phase, either in saturated or in unsaturated conditions, for saturated conditions see Fig. 6.

In this contribution the Bishop type effective stress

$$\boldsymbol{\sigma}' = \boldsymbol{\sigma} + (p_g - \chi(p_g - p_l))\mathbf{1} \tag{27}$$

is employed, whereas the Bishop parameter χ is assumed to equal the saturation of the liquid phase $\chi = S_l$. The weighted pore pressure p is subtracted from the effective stress so that the 2^{nd} Piola Kirchhoff stress tensor, representing the total stress can be split up by

$$\mathbf{S} = \mathbf{F}^{-1}(\tilde{\mathbf{T}}_e - \det \mathbf{F}_s(p_g + S_l(p_l - p_g))\mathbf{1}))\mathbf{F}_s^{-T} \tag{28}$$

with the effective Kirchhoff stress tensor $\mathbf{T}_e^s$ of the solid phase

$$\mathbf{T}_\mathrm{e}^\mathrm{s} = n^B \cdot \mathbf{T}^B + n^F \cdot \mathbf{T}^F \tag{29}$$

evaluated by the macroscopic stresses of the solid components multiplied by the volume fractions respectively. Therefore, an increase in suction induces an additional compressive stress.

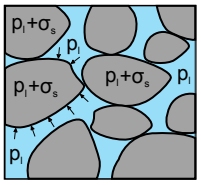

Fig. 6 Concept of effective stresses

3.5 Mechanical behaviour

The model for stress-deformation behaviour includes a novel creep model which combines stress-dependency of creep rate with density-dependency and bases on the models by Ebers-Ernst (2001) and Krase *et al*. (2011). Here the material equations are given and coupling to biochemical degradation and to transport processes is discussed. Focus is laid on degradation-induced settlements.

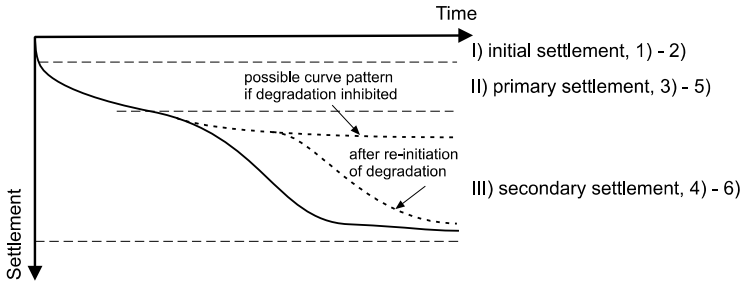

Fig. 7 Settlement pattern of landfills

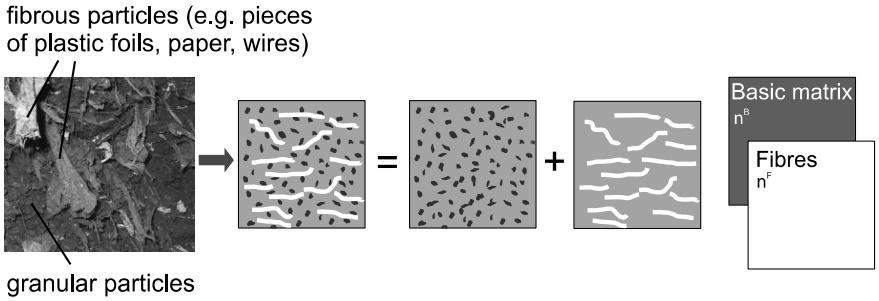

Fig. 8 Two component mechanical model for waste

The stress-deformation behaviour of waste is often compared to that of soils, whereas major differences occur due to the waste's composition and due to its content of degradable particles. Like for general frictional materials, overburden pressure increases the frictional resistance against shearing in the waste's porous skeleton. Furthermore, in experiments a hardening phenomenon is observed as the friction angle tends to increase at high compression, which is attributed to the reinforcing effect of the fibrous particles in the waste. Time dependent settlements have to be covered as well as anisotropies due to emplacement strategies. Stages and mechanisms of settlements may be demonstrated by Fig. 7.

Major phenomena are mechanical effects (distortion, bending crushing, compression of interparticle and intraparticle voids, reorientation) (1), ravelling (movement of fine particles into large voids) (2), consolidation (dissipation of excess pore pressures) (3),creep of waste material (4), physical-chemical effects (corrosion, oxidation, and combustion) (5), and bio-chemical decomposition (6).

The material model treats MSW as a composite in this contribution. Thereby, the solid phase is supposed to consist of a soil-like basic matrix and embedded fibres as shown in Fig. 8.

The basic matrix is made up of the solid, more granular, particles including the pores. The fibres represent the elongate, reinforcing particles like pieces of plastic foils. The material models for both fractions, basic matrix and fibres, are formulated separately, whereas equal displacement fields are assumed. Thus, it is sufficient to consider a single displacement field $\mathbf{u}_S$ for the solid phase only

$$\mathbf{u}^{\mathrm{B}} = \mathbf{u}^{\mathrm{F}} = \mathbf{u}_s \tag{30}$$

with indices *B* denoting the basic matrix and *F* denoting the fibres. Regarding waste, the elastic part of deformations usually is small compared to the inelastic part. Thus, the kinematic description of the coupled model is based on large strain continuum mechanics, but considering large inelastic strains and small elastic strains. This enables strain measures acting on the current configuration.

The model describes compaction of the basic matrix via the effective partial Kirchhoff stress tensor, which is introduced to a highly complex power law. The creep rate $\mathbf{D}_{cr}^{B}$ is defined for

Almansi's strains by the sum of the dyads of the eigenvectors **n** of the effective Kirchhoff stress tensor $\mathbf{T}_e^B$ multiplied by the corresponding creep rate $\dot{\gamma}_{cr,j}^B$

$$\mathbf{D}_{cr}^B = \sum_{j=1}^{3} \dot{\gamma}_{cr,j}^B (\mathbf{n}_{\widetilde{T}_{e,j}^B} \otimes \mathbf{n}_{\widetilde{T}_{e,j}^B}) \tag{31}$$

To cover the influence of degradation on settlements, the approach is directly coupled to decomposition. Two phenomena, compaction caused by load induced distortion of the solid particles themselves as well as due to compression and structural change of the pore space and by change of density due to degradation described by variation of dry solid bulk density $\rho_{s,i}$ are covered by the model presented here

$$\begin{aligned}
\dot{\gamma}_{cr,j}^B &= f_1(\mathbf{T}_e^B)\, f_2(\rho_{s,i}, \mathbf{T}_e^B) \\
f_1(\mathbf{T}_e^B) &= -A_{cr} \left(\frac{\left\langle -\mathbf{T}_{e,jj}^B \right\rangle}{\sigma_0} \right)^{n_{cr}} \\
f_2(\rho_{s,i}, \mathbf{T}_e^B) &= \left[\mathrm{In} \left(\frac{\rho_{\mathrm{s},\infty}}{\rho_{\mathrm{s},\infty} - \rho_{s,i}} \right) \right]^{-p} \cdot \mathrm{In} \left(\frac{\rho_{\mathrm{s}},\mathrm{max}}{\rho_{s,i}} \right)^{p} \\
\rho_{\mathrm{s},\infty} &= \frac{b_{cr}\rho_{s,\min} + \left| \sum_{j=1}^{3} \left\langle -\mathbf{T}_{e,jj}^B \right\rangle \right|^{a_{cr}} \rho_{s,\max}}{b_{cr} + \left| \sum_{j=1}^{3} \left\langle -\mathbf{T}_{e,jj}^B \right\rangle \right|^{a_{cr}}}
\end{aligned} \tag{32}$$

The parameter σ_0 serves for normalization, the parameters A_{cr} and n_{cr} control the stress dependency. The density $\rho_{s,\infty}$ is the maximum density under a certain stress level, covered by the parameters a_{cr} and b_{cr}. It is interpolated between the minimum density $\rho_{s,min}$ and the maximum density $\rho_{s,max}$ dependent on stress.

Time-independent irreversible deformations covered by a cone-shaped yield surface describing resistance against shearing are introduced as well as reversible elastic strains, nevertheless both parts are not relevant for the description of the coupled processes. However, experiments show that water content may reduce total shear strength. Therefore, a simple linear relationship for angle of internal friction dependent on saturation is introduced. Details of the mechanical model for the matrix as well as for the fibres are given in Krase *et al*. (2011).

4. Solution of the coupled initial boundary value problem

Interactions of deformable porous media and fluids are counted among the multi-field problems. In the presented model, the macroscopic description within the Theory of Porous Media leads, together with the constitutive relations, to a set of nonlinear coupled integral formulations of

balance equations, whereby several physical fields are coupled via conjugated state variables in a volume coupled formulation over the domain of a REV.

4.1 Discretization of balance equations

A combination of the Finite-Element method and a node-centered Finite-Volume Method in an ALE formulation is applied for spatial discretization of the governing physical fields. The Backward Euler method is applied for discretization in time.

The Principle of Virtual Work in its Total Lagrangian form, as given by Eq. (6), is discretized by a Bubnov-Galerkin Finite-Element approximation. Thereby, the same set of shape functions **N** is used both for displacements **u** and virtual displacements $\delta\boldsymbol{u}$

$$\mathbf{u} = \sum_i (\hat{u}_i \cdot N_i) \text{ and } \delta\mathbf{u} = \sum_i (\delta\hat{u}_i \cdot N_i) \tag{33}$$

with i as counters over finite element nodes. Discrete quantities are denoted by (^). In this contribution, an isoparametric finite element concept with 9 nodes is used. Correspondingly, quadratic shape functions describe both the displacement field and the element geometry.

The discrete integral forms of the mass balances are obtained from the node-centered Finite-Volume Method (also called Box method) as described by Huber and Helmig (2000). The method is also termed subdomain collocation finite volume method. The approach may be derived from a weighted residual approximation whereas linear shape functions are used. The constant test functions are equal to unity over the domain of a box. The box grid is derived from the finite element mesh, whereas the corner nodes of the finite element mesh are the centers of the boxes. The corner nodes of a box are formed by the centers of adjacent finite elements and by the midpoints of their edges. The element concept is shown in Fig. 9.

The derivation of the discrete form is explained in detail by Huber and Helmig (2000) and extended straightforward to a moving reference frame. Together with a mass lumping of the storage terms the discrete form of Eq. (9) for box i yields

$$\frac{\hat{\rho}_i^{a,t+1} \cdot dV_i^{t+1} - \hat{\rho}_i^{a,t} \cdot dV_i^{t}}{\Delta t} + \int_S \left(\hat{\rho}_U^{\alpha} (\hat{\mathbf{v}}_\pi - \hat{\mathbf{v}}_s) \cdot \mathbf{n} \right)^{t+1} dS = \hat{r}_i^{a,t+1} \cdot dV_i^{t+1} \tag{34}$$

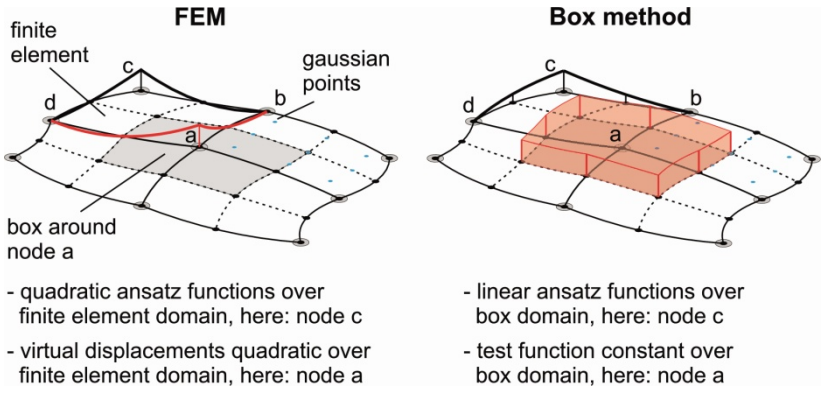

Fig. 9 Shape functions and test functions for FEM and Box method

The density $\hat{\rho}_i^{\alpha,t+1}$ is the partial density of α at the center node of box *i*. The density $\hat{\rho}_U^{\alpha}$ is the upstream density at the surface of box *i*. For stabilization of the convective terms, a fully upwinding is used. The node-centered Finite-Volume method is a conservative scheme, as the rate of change of a conservative variable is balanced by fluxes over the boundaries of a control volume.

The consideration of all components described in Fig. 3 requires the solution of six mass balance equations. Additionally, the balance of energy is formulated to describe instationary temperature fields. The detailed mass balance equations and the equation for conservation of energy are based on the general integral form derived in section 2 including terms due to sources and sinks resulting from biochemical reactions.

4.2 Iterative solution

Different strategies exist to solve coupled problems. Weak and strong coupling or partitioned and simultaneous solution procedures work either with staggered or monolithic strategies. Here a simultaneous solution algorithm is proposed due to the strong interaction between the different physical fields.

The resulting non-linear system of discretized equations is solved by means of the Newton-Raphson method, which yields the tangent matrix $\mathbf{K}_T$. The submatrices of the equation system obtained are visualized by Fig. 10.

Liquid pressure and gas saturation are chosen as state variables of multiphase flow, which is known as pressure-saturation formulation. For the balance equations of degradation and heat generation, the mass fraction of methane in the gas phase, w_g^{CH4}, the mass fraction of acetic acid in the liquid phase w_l^{Ac}, the temperature θ, the partial density of organic matter ρ^{DO} and the partial density of biomass ρ^{X} are chosen as state variables.

The matrices $\mathbf{K}_{uu}$, $\mathbf{K}_{up}$ and $\mathbf{K}_{uc}$ describe the derivation of the virtual work with respect to the nodal displacements **u** and the state variables **p** and **c** respectively. The internal virtual work is nonlinear with respect to both the kinematics and the material.

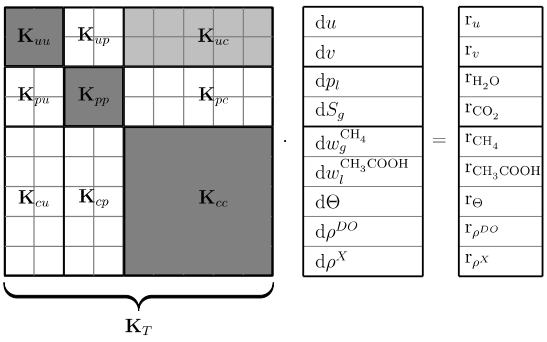

Fig. 10 Linearisation of the discretized equations

The matrix $\mathbf{K}_{up}$ contains the derivation of virtual work with respect to the state variables of multiphase transport. Derivations with respect both to pressure and saturation occur due to the effective stress formulation. Furthermore, the external work of dead loads is coupled to saturation state and liquid density. The matrix $\mathbf{K}_{uc}$ describes dependencies of the virtual work on the state variables of the degradation model. Here the influence of organic and biomass density on creep rate is included. Additionally, external virtual work is affected by change in solid densities.

The Kirchhoff stresses of basic matrix and of the embedded fibres are determined in a local iterative solution of the constitutive evolution equations by the radial return method. The method maps an elastic predictor stress back to the yield surface by a corrector step so that the yield criterion is satisfied at the end of the time-step.

The matrix $\mathbf{K}_{pp}$ describes the two-phasic flow. It considers the influence of gas saturation S_g and liquid pressure p_l on the balance of H_2O and CO_2. The matrix $\mathbf{K}_{cc}$ describes the local reaction processes and physical exchange processes. The matrices $\mathbf{K}_{pu}$ and $\mathbf{K}_{cu}$ contain the derivation of the balance equations with respect to the displacements. Dependency on the deformation arises from the change in size of the control volume. Furthermore, effects from changing porosity and permeability are considered herein. The submatrices $\mathbf{K}_{pp}$, $\mathbf{K}_{pc}$, $\mathbf{K}_{cp}$ and $\mathbf{K}_{cc}$ form the subsystem for description of reactive transport and consider the influence of the corresponding state variables on the balance equations.

5. Analysis of coupled processes

The following examples show the capabilities and characteristics of the developed model in investigations of coupled processes in a landfill structure. Fig. 11 shows the geometry, the boundary conditions and the loading of the analysed virtual landfill.

Exploiting symmetry, only half of the cross section is considered. All analyses are performed for the case of plain strain. Table 3 lists a basic set of initial conditions and parameters. Initial spatial distribution of the solid density over the landfill cross section is assumed to be homogeneous.

The following examples include long-term analyses over periods of up to 30 years. Nodes A, B and C, regarding Fig. 11 are referred to when discussing the results of the simulations.

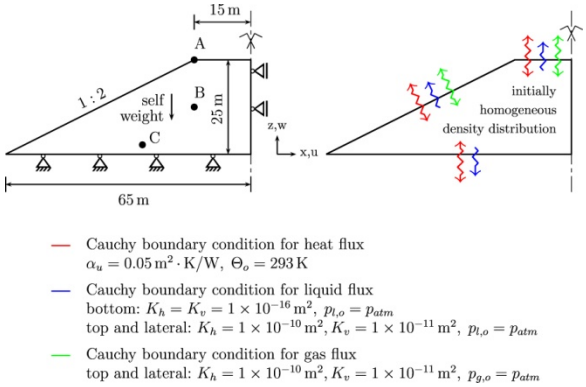

Fig. 11 Geometry, boundary and initial conditions for analysis of a landfill structure

Table 3 Basic set of parameters and initial conditions for landfill structure

Initial conditions			
Saturation	$S_l = 0.65$	Organic matter	$\rho_s^{DO} = 100$ kg/m^3
Dry density	$\rho_s = 500$ kg/m^3	Inert matter	$\rho_s^{IM} = 400$ kg/m^3
K_h	4.5×10^{-11} m^2	Biomass	$\rho_s^{X} = 6 \times 10^{-2}$ kg/m^3
K_v	4.5×10^{-12} m^2	Acetic acid	$w_l^{Ac} = 1.0 \times 10^{-8}$
Liquid pressure	$p_l = p_{atm}$ $p_l = p_{atm}$	Methane	$w_g^{CH_4} = 2.5 \times 10^{-3}$
		Temperature	Θ =303 K
Parameters for creep model		Parameters of degradation model	
ρ_{min}	500 kg/m^3	Hydrolysis rate	$\mu_{\max.R1} = 5 \times 10^{-7} s^{-1}$
$\rho_{max} = \widetilde{\rho}_S$	1042 kg/m^3	Methanog. rate	$\mu_{\max.R2} = 4.6 \times 10^{-5} s^{-1}$
A_{cr}	9.22×10^{-5}h^{-1}	Monod const. R1	$K_{s.R1} = 70$ kg/m^3
n_{cr}	0.939	Monod const. R2	$K_{s.R2} = 3$ kg/m^3
p_{cr}	10.11	Heat cond.	$\lambda_s = 1.5 \times 10^{-4}$ kW/(m·k)
a_{cr}	0.5		
b_{cr}	25.55		
Other parameters			
Atm. pressure	$p_{atm} = 1 \times 10^5$ kPa	Fibres content	n^F =0.05
Res. Gas satur.	$S_{g.res}$ = 0.01		

5.1 Influence of temperature on degradation and settlements

The first investigation focuses on the influence of varying temperatures on settlements and degradation over a period of 27 years, regarding an initial organic matter content of 20%. The parameters of the degradation model account for the influence of transient temperatures on degradation rates. Two variants with different heat conductivities of the solid phase are compared. Conductivity is chosen to $\lambda_{s,1}$ = 0.15 W/(m·K) in variant 1 and to $\lambda_{s,2}$ = 1.00 W/(m·K) in variant 2.

Fig. 12 shows the organic density in nodes A and B. After 30% of organic matter is decomposed, degradation stops almost completely as visible from the graphs in Fig. 12. From the evolution of temperature in A and B in Fig. 13, it is obvious that the stop of degradation is due to the quick temperature rise up to Θ = 80°C in B.

At this temperature, the value of the temperature function becomes $f_\Theta \approx 0$ what indicates dying biomass. Temperature is high in the center and approaches the outer temperature of Θ = 20°C mainly because of thermal conduction, Fig. 14. While heat is more and more transported to the outside, temperature slightly decreases to about 70°C. Conditions for degradation improve again and more organic matter is degraded as shown in Fig. 12. An equilibrium stage is reached and temperature is maintained at this level for about 15 years. At the surface node A, degradation proceeds more uniformly due to the constantly lower temperature. Hence, no sudden stop of degradation is observed close to the surface.

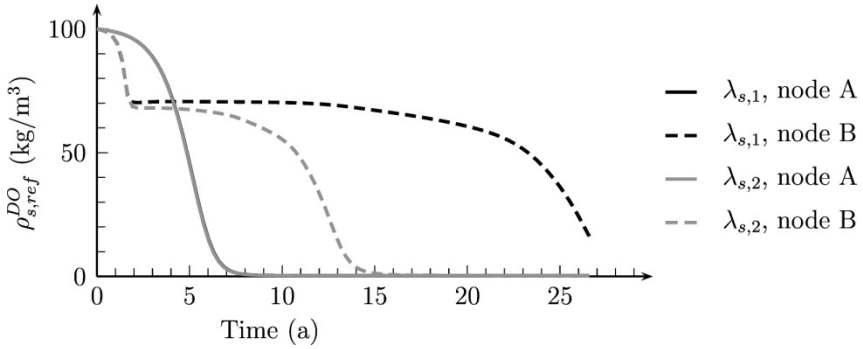

Fig. 12 Partial density of organic matter at different nodes

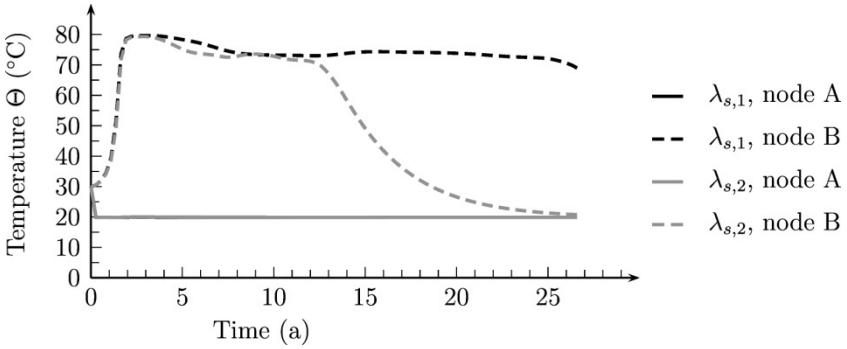

Fig. 13 Temperature evolution at nodes A and B

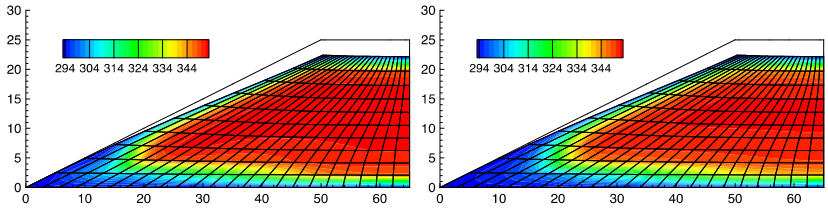

(a) Θ (K) at $t = 2.2$ a, $\lambda_{s,1}$

(b) Θ (K) at $t = 2.2$ a, $\lambda_{s,2}$

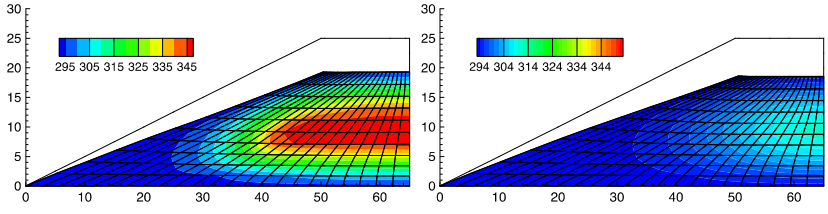

(c) Θ (K) at $t = 18.6$ a, $\lambda_{s,1}$

(d) Θ (K) at $t = 18.6$ a, $\lambda_{s,2}$

Fig. 14 Distribution of temperatures

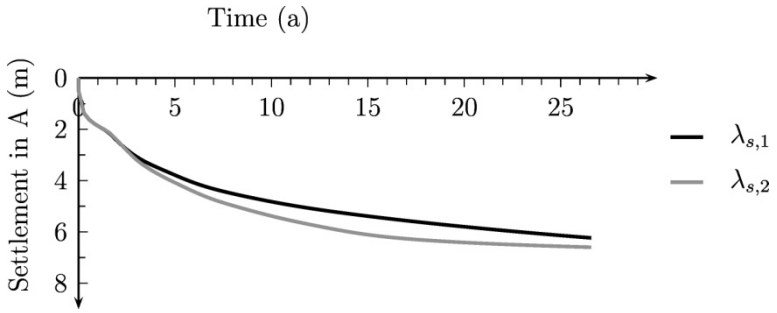

Fig. 15 Time-settlement curves for different heat conduction coefficients

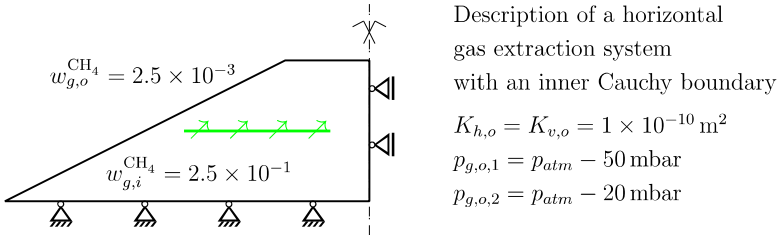

Fig. 16 Horizontal gas extraction system

The contour plots of temperature at different times in Fig. 14 show that increased heat is present over a broader area of the landfill for the material with lower heat conductivity. The example shows that the model may describe the temperature evolution in landfills but it is highly recommended to employ reliable data on heat conductivity and degradation rates.

Settlements differ mainly in the interim stage between 10 years and 20 years, see Fig. 15, with a maximum difference of 1 m related to a total height of 25 m. Thus, the large settlements of about 20% are varied to about 4% in addition depending on the heat conductivity coefficient employed. Temperature rise is supposed to be overestimated by the model considering the temperature measurements on site by Mora Naranjo (2004). The overheating is a combined effect of maximum degradation rate, the temperature influence on degradation rates and the heat conductivity of the waste mixture.

5.2 Analysis of a gas extraction system

Along with the anaerobic biological degradation of organic matter, landfill gas is produced. It is composed of carbon dioxide and methane mainly. The landfill gas can be collected and flared or, if possible, utilized in a gas engine to generate power. Simultaneously, harmful impacts on climate may be reduced. A crucial point is usually the estimation of gas volume and its composition. If the fraction of the originary landfill gas is too low, the engine cannot be run effectively. Hence, tools for designing landfill gas extraction systems are of avail for landfill operators.

To describe an active gas extraction at the landfill model investigated here, an inner Cauchy boundary condition is employed. It is assumed that the extraction pipe is placed exactly horizontally as shown in Fig. 16, whereas, in practice the pipes would be emplaced with a slight slope to separate condensate. The analysis is performed for an initial organic matter content of 20 %.

The gas phase of the developed model comprises only carbon dioxide, methane and vapor as components. To distinguish the air within the landfill from the outer air initially, the mass fraction of methane is set to a very low value of $2.5 \cdot 10^{-3}$ outside the landfill whereas it is high within the landfill. The intended purpose is to have an indicator on whether air from outside is sucked into the landfill body. When operating an active gas extraction system this is usually tried to avoid. The soaking of extraneous air might lead to aerobic conditions so that less methane is produced and the effectiveness of the engine is reduced. Hence, a low applied vacuum is usually chosen. It should, however, be of such magnitude that as less landfill gas as possible leaves the landfill body by diffuse emissions over the surface. Here, two cases are compared in the simulations, see Fig. 16. The permeability of the waste is $K_h = 1 \cdot 10^{-12}$ m^2 and $K_v = 1 \cdot 10^{-13}$ in this example. At $t = 2.2$ years $= t_E$ the extraction system is activated. The simulations are performed under isothermal conditions at $\Theta = 303$ K to ensure uniform degradation. For case $p_{g,o,1}$ two variants are compared to investigate the influence of deformation on gas flow. Variant 1 assumes $\kappa_\phi = 1.0$ in Eq. (23), whereas variant 2 assumes $\kappa_\phi = 10.0$ implying a higher decrease in permeability in variant 2 due to compaction.

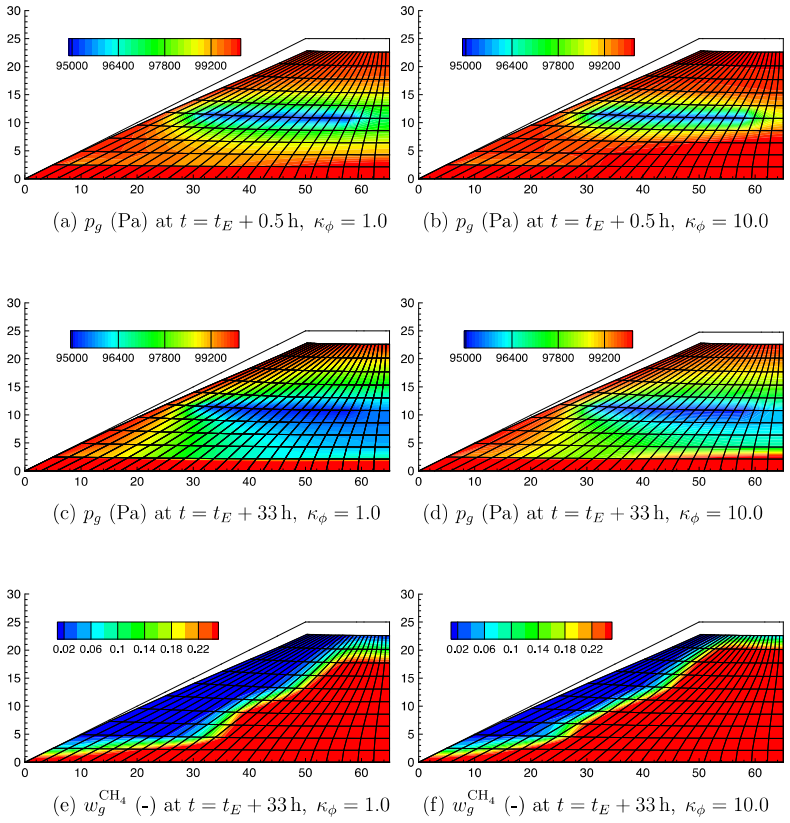

(a) p_g (Pa) at $t = t_E + 0.5$ h, $\kappa_\phi = 1.0$ (b) p_g (Pa) at $t = t_E + 0.5$ h, $\kappa_\phi = 10.0$

(c) p_g (Pa) at $t = t_E + 33$ h, $\kappa_\phi = 1.0$ (d) p_g (Pa) at $t = t_E + 33$ h, $\kappa_\phi = 10.0$

(e) $w_g^{\mathrm{CH_4}}$ (-) at $t = t_E + 33$ h, $\kappa_\phi = 1.0$ (f) $w_g^{\mathrm{CH_4}}$ (-) at $t = t_E + 33$ h, $\kappa_\phi = 10.0$

Fig. 17 Distribution of gas pressure and methane fraction after initiation of gas extraction

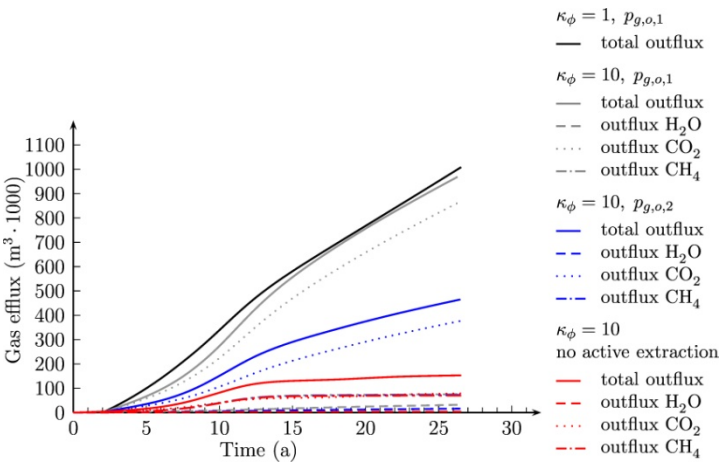

Fig. 18 Efflux of gas

Fig. 17 shows the spatial distribution of gas pressure for the two variants. At Δt = 0.5 h after activation of gas collection, the effect of gas extraction is already visible from the negative pressure close to the extraction pipe in Figs. 17(a) and 17(b). The vacuum propagates faster for κ_ϕ= 1.0 due to the higher permeability upon deformation. After Δt = 33 h a larger area of the landfill cross section is under negative pressure, compare Figs. 17(c) and 17(d). In the center zone, the pressure is lower over a larger area in case of κ_ϕ= 1.0.

The contour plots of methane fraction in Figs. 17(e) and 17(f) show that air is sucked in from outside and that is has infiltrated deeper into the landfill for the case with higher permeability κ_ϕ = 1.0 than for κ_ϕ = 10.0 after Δt = 33 h. The Figures also show that the extraneous air spreads faster in horizontal than in vertical direction due to the higher horizontal permeability.

Fig. 18 compares the cumulative out flux of gas over the entire simulation period of 27 years for the investigated variants. For case 1, $p_{g,o,1}$, about $1 \cdot 10^6$ m^3 gas are extracted after 27 years, which is within a realistic range. In case of $p_{g,o,2}$ the extracted volume is accordingly less.

In case 1, only less than 10% of the collected gas is methane. The reason for not obtaining a ratio close to the typical ratio of 60% to 40% is the limited gas composition that can be described by the model. The extraction is switched on after Δt = 2.2 years. As shown in Figs. 17(e) and 17(f) outer air is sucked in. This air has a low methane content and thus a high CO_2 content. The outer air affects the composition of the extracted gas volumes in the observed manner. This is proven by analyzing case 2. The extracted volume of methane is nearly the same, but the volume of CO_2 has considerably decreased, it is less than 50% as in case 1. A comparative analysis without an inner gas extraction system gives ratios of about 50% of methane and 50% of carbon dioxide. From the obtained gas production curve it is obvious that gas production is strongly related to degradation.

The effect of deformation on hydraulic parameters is relatively low in the given example, but nevertheless it is concluded that its influence has to be kept in long-term modeling of landfills. As porosity is related to density, also the change of permeability due to change in solid mass is considered, e.g., biofilm growth.

6. Conclusions

The presented model describes the coupled THMC processes by means of a complex continuum mechanical approach. Prognosis of long-term behaviour of landfill structures can be investigated seriously only by considering the coupling of the most important processes on the landfill-site as well as the different scales in space and time to be observed. Balance equations of momentum, mass and energy consider stress deformation behaviour, transport phenomena and biochemical reactions. Better understanding of the coupled processes due to numerical analysis may improve the possibility to control actively the most important properties. The applications indicate the capabilities of the model, which may be enhanced by further phenomena, if necessary.

It is concluded that in further extensions of the model additional gas components to describe ambient air, i.e. nitrogen and oxygen may be included. Additionally, the degradation model may be supplemented by an aerobic pathway, although only the outer shell of a landfill, which corresponds to about 0.3 m, might be affected by aerobic degradation. A surface oriented description could be a numerical efficient possibility to incorporate this phenomenon. Furthermore, the model could be applied to describe aerobic degradation from artificial aeration.

Last but not least the model is to be extended to 3D and the model parameters are to be determined by investigations of experiments and landfill-site data for modeling realistic landfill-site situations. Probably the consideration of stochastic data would support evaluation of the numerical results. Then, landfill prognosis could be investigated more realistically.

Acknowledgments

The research described in this paper was developed within the Collaborative Research Centre *SFB 477 – Life Cycle Assessment of Structures via Innovative Monitoring* and financially supported by German Research Foundation.

References

de Boer, R. (2005), *Trends in continuum mechanics of porous media*, Springer.

Bowen, R. (1976), *Continuum physics. Theory of Mixtures*, (Ed. Eringen, A.), Acad. Press New York.

Brooks, R.H. and Corey, A. (1966), "Properties of porous media affecting fluid flow", *J. Irrig. Drain. Div.*, **92**(IR2), 61-88.

Burdine, N. (1953), "Relative permeability calculations from pore-size distribution data", *Petroleum Transactions AIME*, **198**, 71-78.

Durmusoglu, E., Corapcioglu, M.Y. and Tuncay, K. (2005), "Landfill settlement with decomposition and gas generation", *J. Environ. Eng. - ASCE*, **131**(9), 1311-1321.

Donea, J., Huerta, A., Ponthot, J. and Rodriguez-Ferran, A. (2004), "Arbitrary Lagrangian-Eulerian methods", *Encyclop. Comput. Mech.*, **1**, 1-25.

Ebers-Ernst, J. (2001), *Modellierung des Inelastischen Verformunsverhaltens von Siedlungsabfalldeponien*, Ph.D. Thesis, Institut für Statik, Braunschweig.

Elagroudy, S.A., Warith, M.A. and Ghobrial, F.H. (2008), *Solid waste settlement in landfills/bioreactor landfills, in: waste management research trends*, Nova Science Pub Inc.

El-Fadel, M., Findikakis, A. and Leckie, J. (1996a), "Numerical modeling of generation and transport of gas and heat in landfills I. model formulation", *Waste Manage. Res.*, **14**(5), 483-504.

El-Fadel, M., Findikakis, A. and Leckie, J. (1996b), "Numerical modeling of generation and transport of gas

and heat in sanitary landfills II. model application", *Waste Manage. Res.*, **14**(6), 537-551.
El-Fadel, M. and Khoury, R. (2000), "Modelling settlement in msw landfills: a critical review", *Crit. Rev. Env. Sci. Tech.*, **30**(3), 327-361.
Garcia de Cortazar, A.L., Lantaron, J.H., Fernandez, O.M., Monzon, I.T. and Lamia, M.F. (2002a), "Modelling for environmental assessment of municipal solid waste landfills (Part I: Hydrology)", *Waste Manage. Res.*, **20**(2), 198-210.
Garcia de Cortazar, A.L., Lantaron, J.H., Fernandez, O.M., Monzon, I.T. and Lamia, M.F. (2002b), "Modelling for environmental assessment of municipal solid waste landfills (Part II: Biodegradation)", *Waste Manage. Res.*, **20**(6), 514-528.
vanGenuchten, M. (1980), "A closed-form equation for predicting the hydraulic conductivity of unsaturated 6soils", *Soil Sci. Soc. Am. J.*, **44**(5), 892-898.
Haarstrick, A., Hempel, D.C., Ostermann, L., Ahrens, H. and Dinkler, D. (2001), "Modelling of the biodegradation of organic matter in municipal landfills", *Waste Manage. Res.*, **19**(4), 320-331.
Hettiarachchi, C.H., Meegoda, J.N., Tavantzis, J. and Hettiaratchi, P. (2007), "Numerical model to predict settlements coupled with landfill gas pressure in bioreactor landfills, *J. Hazard. Mater*., **139**(3), 514-522.
Huber, R. and Helmig, R. (2000), "Node-centered finite volume discretizations for the numerical simulation of multiphase flow in heterogeneous porous media", *Computat. Geosci.*, **4**, 141-164.
Ivanova, L. (2007), *Quantification of factors affecting rate and magnitude of secondary settlement of landfills*, Ph.D. Thesis, School of Civil Engineering and the Environment, Southampton.
Kindlein, J., Dinkler, D. and Ahrens, H. (2006), "Numerical modeling of multiphase flow and transport processes in landfills", *Waste Manage. Res.*, **24**(4), 376-387.
Krase, V., Kowalsky, U., Bente, S., Dinkler, D. (2009), "Coupling Biodegradation models of varying complexity with transport processes in landfills", Proceedings of the *12th Intern. Waste Man. and Landfill Symp.*, Sardinia.
Krase, V., Bente, S., Kowalsky, U. and Dinkler, D. (2011), "Modelling the stress deformation behaviour of municipal solid waste", *Géotechnique*, **61**(8), 665-675.
Lewis, R. and Schrefler, B.A. (1998), *The finite element method in the static and dynamic deformation and consolidation of porous media*, John Wiley & Sons.
Lobo, A., Lopez, A., Cobo, N. and Tejero, I. (2008), "Simulation of municipal solid waste reactors using MODUELO", *Waste Resour. Manage*., **161**(3), 99-104.
Machado, S., Vilar, O. and Carvalho, M. (2008), "Constitutive model for long term municipal solid waste mechanical behavior", *Comput. Geotech.*, **35**(5), 775-790.
McDougall, J. (2007), "A hydro-bio-mechanical model for settlement and other behaviour in landfilled waste", *Comput. Geotech.*, **34**, 229-246.
Monod, J. (1949), "The growth of bacterial cultures", *Annu. Rev. Microbiol.*, **3**, 371-394.
Mora-Naranjo, N. (2004), *Analyse und Modellierung anaerober Abbauprozesse in Deponien*, Ph.D. Thesis, Technische Universität Carolo-Wilhelmina zu Braunschweig.
Mualem, Y. (1976), "A new model for predicting the hydraulic conductivity of unsaturated porous media", *Water Resour. Res.*, **12**, 513-522.
Powrie, W. and Beaven, R.P. (1999), "Hydraulic properties of household waste and implications for landfills", *Proceedings of the Institution of Civil Engineers, Geotechnical Engineering*.
Oweis, I.S. (2006), "Estimate of landfill settlements due to mechanical and decompositional processes", *J. Geotech. Geoenviron*., **132**(5), 644-650.
Park, H. and Lee, S. (2002), "Long-term settlement behaviour of MSW landfills with various fill ages", *Waste Manage. Res*., **20**, 259-268.
Reichel, T. and Haarstrick, A. (2008), "Modelling decomposition of MSW using genetic algorithms", *Waste Resour. Manage*., **161**(3), 113-120.
Ricken, T. and Ustohalova, V. (2005), "Modeling of thermal mass transfer in porous media with applications to organic phase transition in landfills, *Comput. Mater. Sci.*, **32**, 498-508.
Ricken, T., Robeck, M. and Widmann, R. (2009), "A 3D-finite element simulation of biological conversion processes in landfills using a multiphase model based on the theory of porous media", Proceedings of the

12th International Waste Management and Landfill Symposium, Sardinia, Italy.
Simoes, G. and Da Silva, F. (2011), "Calibration of a coupled mechanical and biological model for landfill settlement prediction based on field monitoring data", *Proceedings of the 4th International Workshop Hydro-Physico-Mechanics of Landfills*, Santander, Spain.
Ustohalova, V., Ricken, T. and Widmann R. (2006), "Estimation of landfill emission lifespan using process oriented modeling", *Waste Manage*., **26**(4), 442-450.
Wall, D. and Zeiss, C. (1995), "Municipal landfill biodegradation and settlement", *J. Environ. Eng. - ASCE*, **121**, 214-223.
White, J. (2008), "The application of ldat to the hpm2 challenge", *Waste Resour. Manage.*, **161**(4), 137-146.
Yu, L., Batlle, F., Carrera, J. and Lloret, A. (2009), "Gas flow to a vertical gas extraction well in deformable MSW landfills", *J. Hazard. Mater*., **168**(2-3), 1404-141.